Chapter 2. Experiment

2.1 Radiation sources

The experimental setup consists of a radiation source delivering radiation beams incident on the targets under investigation, a vacuum chamber for performing experiments, in-situ and ex-situ instrumentation for analyses.

The main radiation source is a Chirped-Pulsed-Amplification (CPA) based Ti: Sapphire femtosecond laser system that includes a Spectra Physics Ti: Sapphire self-mode locking oscillator (repetition rate 82 MHz, pulse duration 100 fs, pulse energy on the order of nJ, central wavelength 800 nm with limited tunability; 1W-average power, stability better then 5%) pumped by a continuous, multiline Ar^+ laser.

The femtosecond seed pulse (a nearly transform-limited pulse) is stretched to 100 ps and directed into a frequency doubled Nd: YLF pumped regenerative Ti: Sapphire amplifier and amplified at about 500 µJ by the CPA technique.

The amplified pulse is then compressed to 200 fs. The CPA technique allows one to modify the pulse duration from 200 fs to up to 10 ps, while maintaining the other parameters [Var99], by controlled misalignment of the compressor This is done by modifying the distance between the compression gratings so that the chirp remains partially uncompensated. The temporal profile (Gaussian) of the pulse has a good quality, the satellite impulses are negligible and the contrast between the main pulse and the background is better than 10^3:1. Pulse duration was measured with a second harmonic autocorrelation setup. The repetition rate can be varied between 100 Hz and 1 kHz. A mechanical shutter synchronized with the laser (with the Pockels Cell driver) is used as a pulse picker, allowing a controlled number of pulses to irradiate the sample. The laser beam was focused by a quartz lens (f=75 mm) onto the sample surface, leading to a focus area[1] (at $1/e^2$) of ~ 680µm^2. Energy attenuation was done using calibrated neutral filters and measured with a LTB pyroelectric measuring head. The unfocused beam is linearly polarized and has a Gaussian spatial profile with a diameter of 2.8 mm (FWHM).

[1] For the 100 fs laser system (Clark MXR) the focal spot was 470 µm^2 due to a larger aperture.

Other radiation sources include similar systems, an IR Clark oscillator-regenerative amplifier system with pulse duration of 100 fs, energies per pulse up to 600 µJ, and a multipass amplifier system with pulse duration below 50 fs.

The samples are situated in a vacuum chamber allowing pressures down to 10^{-6} mbar (pumped by a combination of membrane and turbomolecular pumps).

The sample positioning system is a precision *x-y* translation stage driven by computer controlled stepper motors. The samples were supported on a metal target holder such that the laser-processed area was not backed.

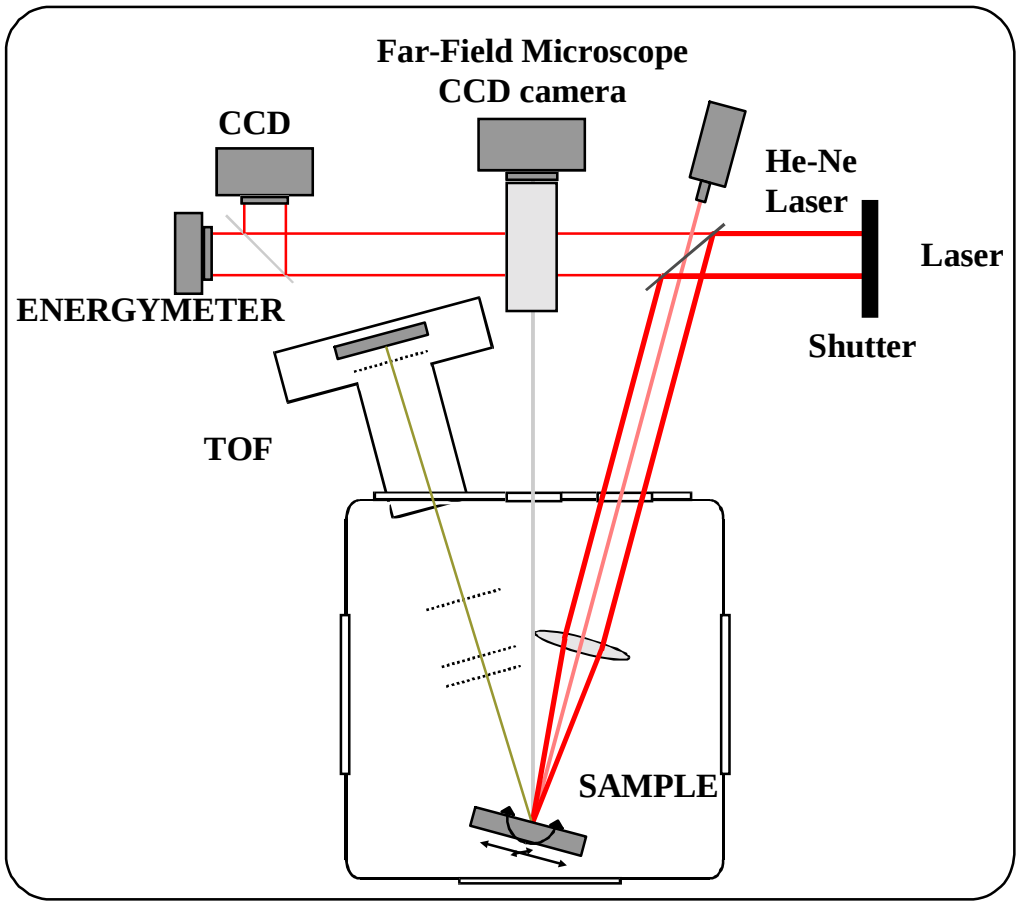

Fig. 2.1-1 Overall view of the experimental setup.

The chamber allows multiple detection facilities at different viewing angles. Time-of-flight (TOF) particle detection based on a linear TOF mass spectrometer was one of the most important facilities, and most of the experimental results were obtained from TOF measurements with angle resolution. Part of the work done in the framework of this thesis involved the upgrade of an ion TOF spectrometer to allow detection of neutrals and electrons.

An overview of the setup is given in Fig. 2.1-1. More details concerning the general arrangement and also the electronics are given in [Var99].

Fig. 2.1-2 outlines schematically the TOF experimental arrangement. The angle between the TOF detector axis and the laser direction was kept constant during the experiment at 25°. To determine the angular distribution the sample was rotated in the incidence plane with respect to the TOF axis so that the angle between the laser and the target was dynamically adjusted. The rotation axis, contained in the sample surface plane, is perpendicular to the plane defined by the laser direction and the TOF axis (the incidence plane). In this way the normal to the surface plane at the point of laser impact will sweep the incidence plane. All angles are given with respect to the surface normal and TOF axis. The laser fluence was corrected to the same values for all the angles according to the following formula.

$$F(\theta) = F(0)/\cos\theta$$

where *F(0)* is the laser fluence at normal incidence.

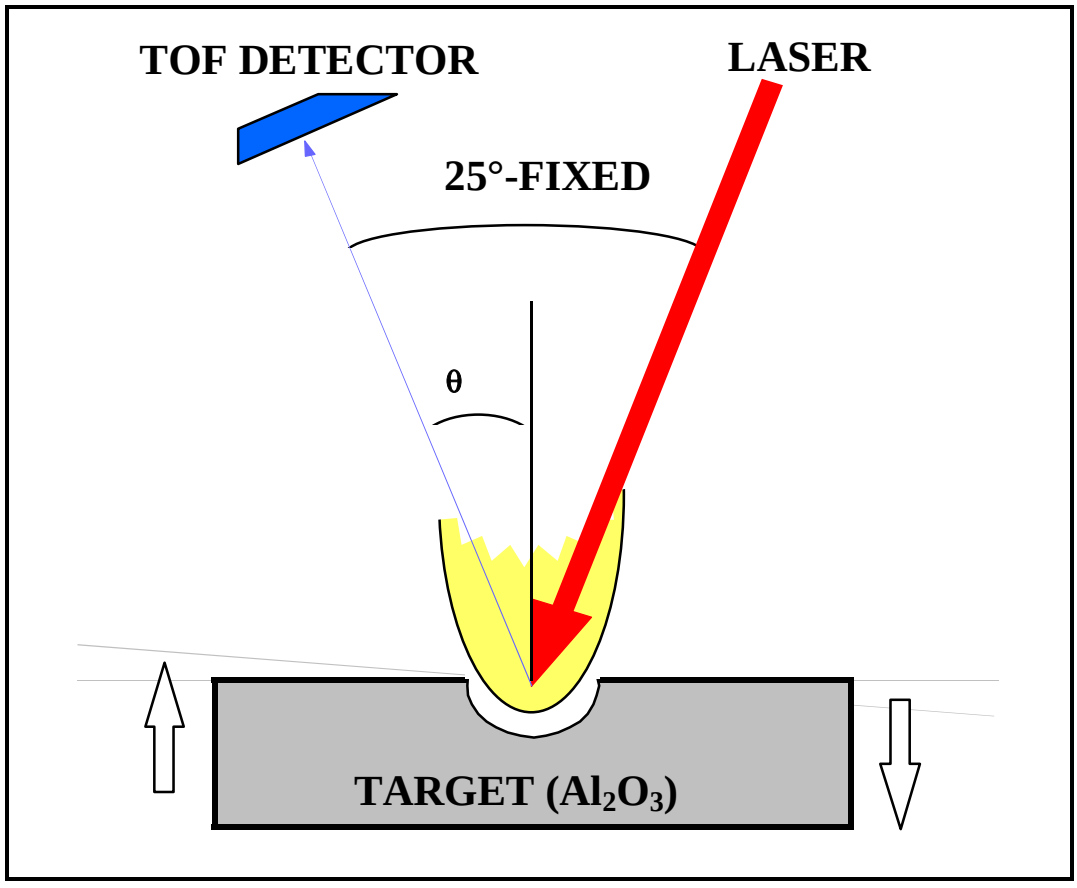

Fig. 2.1-2 TOF experimental arrangement. It should be noted that the angle between the TOF detector axis and the laser was fixed at 25°. The angle of incidence varied during the target rotation (the arrows indicate the direction of rotation, the rotation axis being perpendicular to the figure plane in the point of laser impact).

The sample surface and the irradiated zone were monitored online with a combination of far-field microscope and a CCD camera. A He-Ne laser was used for alignment purposes.

2.2 Mass spectrometry and TOF detection

TOF apparatus

The primary goal of the in-situ TOF measurements was the determination of the masses and velocities of the ablated particles under different ablation conditions. For the velocity distributions two geometries were investigated. The TOF detector axis was fixed normal to the sample surface (laser at 25° incidence) to allow on axis measurements or the laser was adjusted for normal incidence with off-axis TOF detection. This enables either fast particle detection (the top central part of the plume) but with a shifting of the plume towards the laser direction and thus less efficient particle detection as a crater is formed, or secondly a constant alignment of the plume with respect to the laser and the TOF detector but with only off-axis emitted particles being detected.

Positively charged Al^+ and O^+ ions, Al neutrals and electrons were measured by a linear TOF mass spectrometer based on the Wiley-McLaren configuration [Var99] (Fig. 2.2-1). As seen in Fig. 2.2-1, the ions were allowed to drift for 65 mm and then extracted into the mass spectrometer with a pulsed electric field applied to the extraction zone, and detected with a microsphere plate (MSP) situated at a distance of 289 mm from the target. The TOF mass spectrometer can be used in two configurations: 1) without pulsed extraction, which allows one to measure the total flux of the particle beam as a function of the drift time from the target to the MSP. Unfortunately mass resolution is almost suppressed in this mode. Nevertheless, different species can be still be distinguished with the help of a retarding field, present in front of the MSP, cutting the low energy particles. The second mode involves a time-controlled pulsed extraction voltage applied to the extraction grids at different delay times with respect to the laser, which allows mass separation for constructing the mass-resolved velocity distribution at the distance of 65 mm from the target. A good example is given in Fig. 2.2-2 showing both non-mass resolved spectra (with a small possibility for a limited mass resolution by applying the retarding field) and the mass resolved spectra for different extraction times.

In the second mode only particles present in the extraction region (1 cm long) at the moment of the pulsed voltage application are detected. All other particles (from outside the extraction region at the moment of voltage appliance) are rejected by either the positive potential of the first grid (which prevents extra particles from entering into the extraction region after the extraction pulsed was applied) or by the retarding field (which removes particles already present in the acceleration region at the moment of applying the voltage;

details will be given below). The voltages applied to the TOF grids are used in such a way that particles of equal mass/charge ratio originating from different positions in the extraction region reach the detector at the same time (double temporal focusing).

This can be expressed by the conditions:

$$\left.\frac{dt}{dk}\right|_{k=1} \approx 0$$

$$\left.\frac{d^2t}{dk^2}\right|_{k=1} \approx 0$$

where t is the arrival time at the detector (a sum of times the particle spent in different regions of the TOF) and k is the relative coordinate in the extraction region ($k=1$ for the middle of the extraction region). Details about the focusing conditions and also the electrical scheme with the triggering conditions can be found in [Var99].

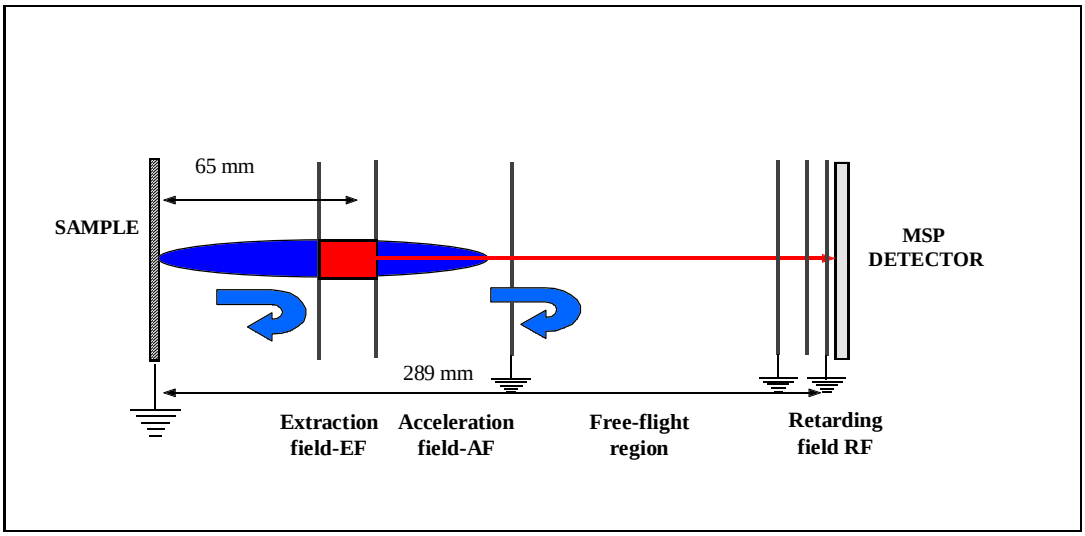

Fig. 2.2-1 Scheme of the Wiley-McLaren linear mass spectrometer.

Typical mass-resolved spectra are given in Fig. 2.2-2 for different extraction times.

As will be shown below, the mass spectrometer extracts particles from a narrow angular range. The velocity distribution of interest is thus defined as $dN/dv=n(v)$ with N [particles/cm] being the total (linear) particle density. This velocity distribution is mapped onto the distance s from the target ($s=vt_0$) as $n(s,t_0)$ where t_0 is the delay between the laser pulse and the applied extraction voltage. Taking into account the position of the extraction region with respect to the sample we can derive a relationship between the particle distribution in velocity space $n(v)$ and the measured ion yield at time t_0 (the total number of ions between the grids at this time).

The ion yield detected at different extraction voltage delay times t_0 (the total number of ions in the extraction region at the moment t_0) can be expressed as:

$$I(t_0) = \int_L^{L+D} n(s,t_0)ds = \int_L^{L+D} \frac{\partial N(s,t_0)}{\partial s} ds = \int_{\upsilon(L)}^{\upsilon(L+D)} \frac{\partial N(s(\upsilon))}{\partial s} \frac{\partial s}{d\upsilon} d\upsilon = \int_{\upsilon(L)}^{\upsilon(L+D)} n(\upsilon)\frac{\partial s}{d\upsilon} d\upsilon$$

$$I(t_0) = n\left(\frac{L+\frac{D}{2}}{t_0}\right)\left(\frac{L+D}{t_0} - \frac{L}{t_0}\right) = n(\upsilon_0)\frac{D}{t_0}$$

where D represents the length of the extraction region and L the coordinate of the extraction region with respect to the sample position, and $n(s, t_0)$ is a (linear) particle density as a function of position s at time t_0.

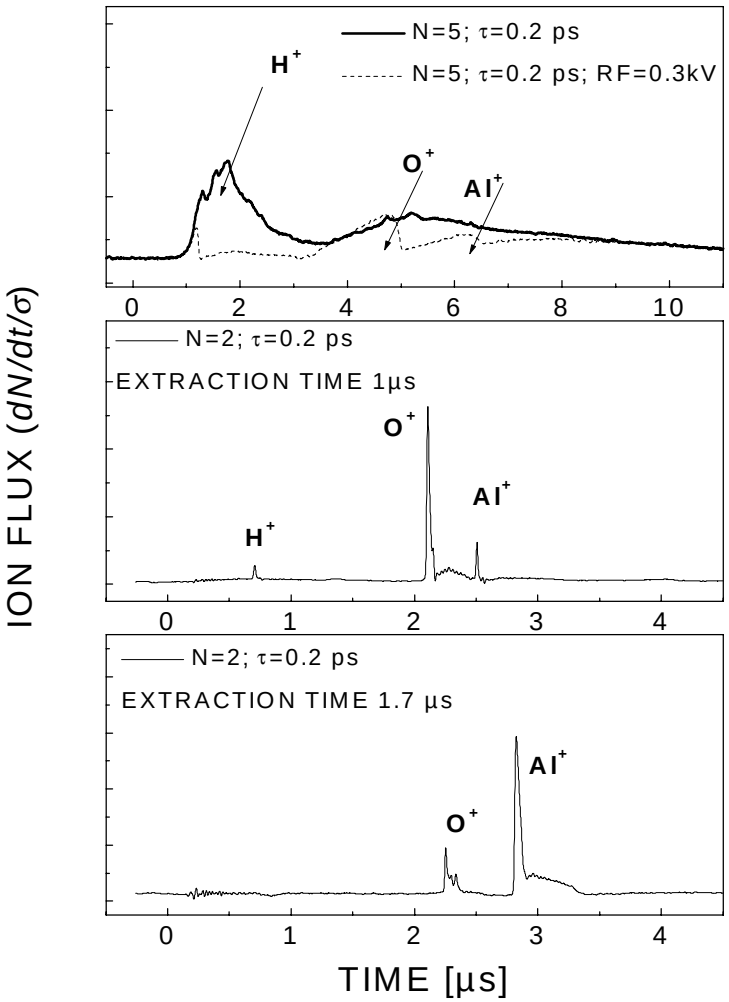

Fig. 2.2-2 Non-mass resolved (top) and mass resolved acquired spectra for Al_2O_3 at different extraction times. For the non-mass resolved spectra, the effect of a retarding field (RF) of 300 V is also visible allowing a certain type of mass discrimination. Pulse duration τ=0.2 ps.

In this way, the ion yield can be expressed as:

$$n(\upsilon) \propto I(t_0) \times t_0$$

Thus, for the velocity distribution, the measured ion yield has to be corrected by multiplying with a factor equal to the extraction time (Jacobi factor).

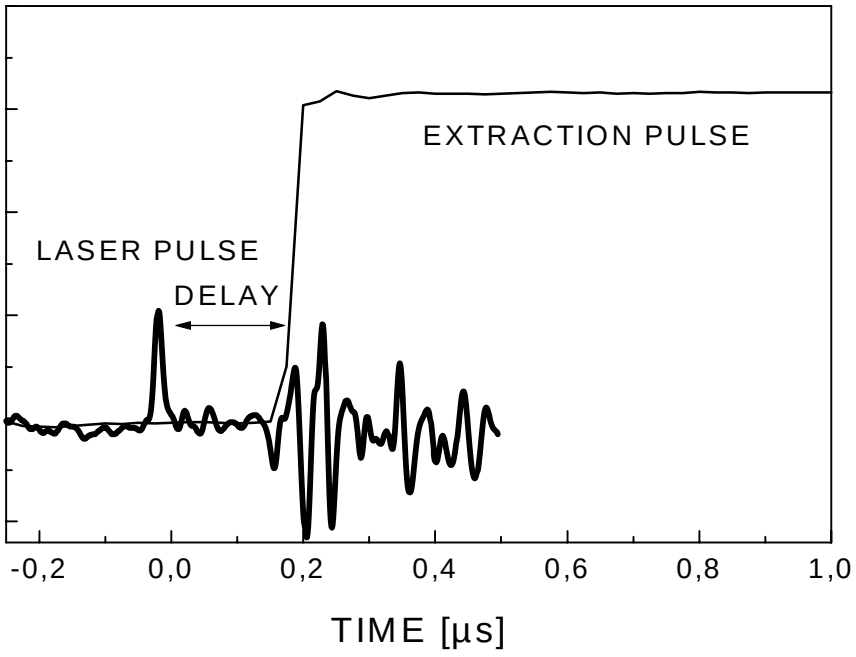

Fig. 2.2-3 Extraction field with respect to the laser pulses. The visible spikes are electrical noise due to the high voltage application.

Voltage adjustments

The voltages for the extraction and the acceleration region were chosen to ensure efficient temporal focusing and good mass resolution. The voltage difference across the extraction region was ~300 V and across the acceleration region was ~1000 V.

To construct the velocity distributions the pulsed extraction field was delayed with respect to the laser pulse to allow particles with different velocities to enter the extraction region. In Fig. 2.2-3 we have depicted both the signal corresponding to the laser pulse recorded with a photodiode and the trace of the applied extraction voltage, delayed with respect to the laser. The electrical noise due to high voltage switching is also visible on the laser trace. In this way it was possible to scan the entire plume by controlling the extraction voltage delay time. To limit the region of the detected particles to the extraction region, a dynamically adjusted retarding field was used to stop particles originating from the

acceleration region. Since we detect ions with different masses or charge states having thus different energies, the retarding field was adjusted for each mass according to the extraction time with respect to their energies at the edge between the acceleration region and the extraction zone. The measured and calculated retarding field values are shown in Fig. 2.2-4 for the case of a sapphire sample (O^+ and Al^+ detection). The measured values for the necessary retarding field represent the stopping values for particles in the acceleration region when no voltage difference is applied across the extraction region. At these values the ion yield (originating from the acceleration region) drops to zero.

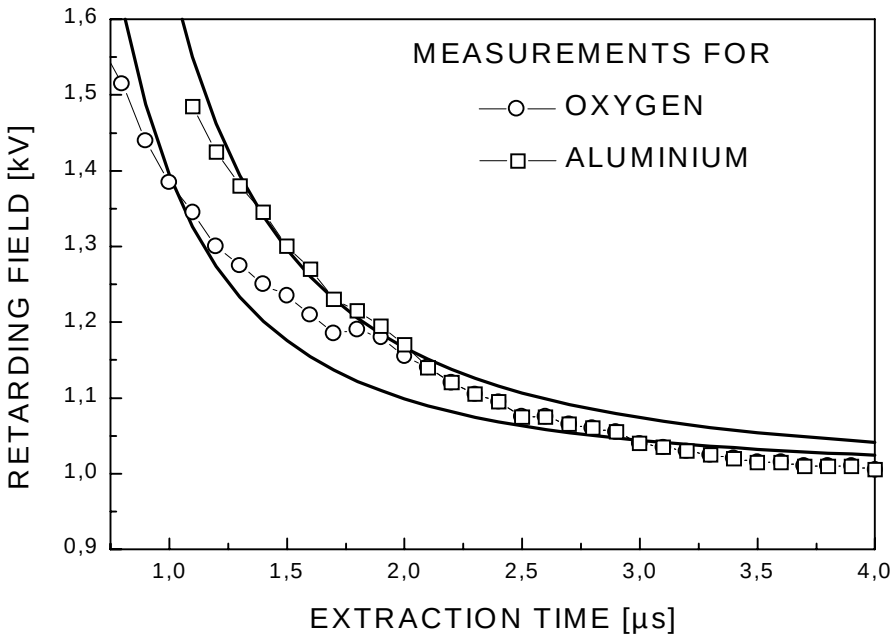

Fig. 2.2-4 Measured (points) and calculated (lines) retarding field (RF) values for different extraction times.

Fig. 2.2-5 shows the simulation of the kinetic energy of O^+ and Al^+ ions (originating from different regions in the TOF at the moment when the extraction pulsed is applied) at the location of the retarding field grid. It illustrates also the values for the retarding field at different delay times for both O^+ and Al^+ species to efficiently remove particles from outside the extraction region. In other words, the retarding field enables particle discrimination according to their point of origin. The coordinates for the extraction region are between 60 and 70 mm. From 70 to 130 mm the particles are situated in the acceleration region. Also the necessary stopping values for the retarding field are depicted. The use of a dynamic retarding field with respect to the masses and extraction times is of crucial importance for constructing

precise velocity distributions. The kinetic energy does not simply decrease as a function of the particles coordinates (equivalent to a less energy gain in the DC electric field) because the initial kinetic energy plays a fundamental role especially for small extraction times.

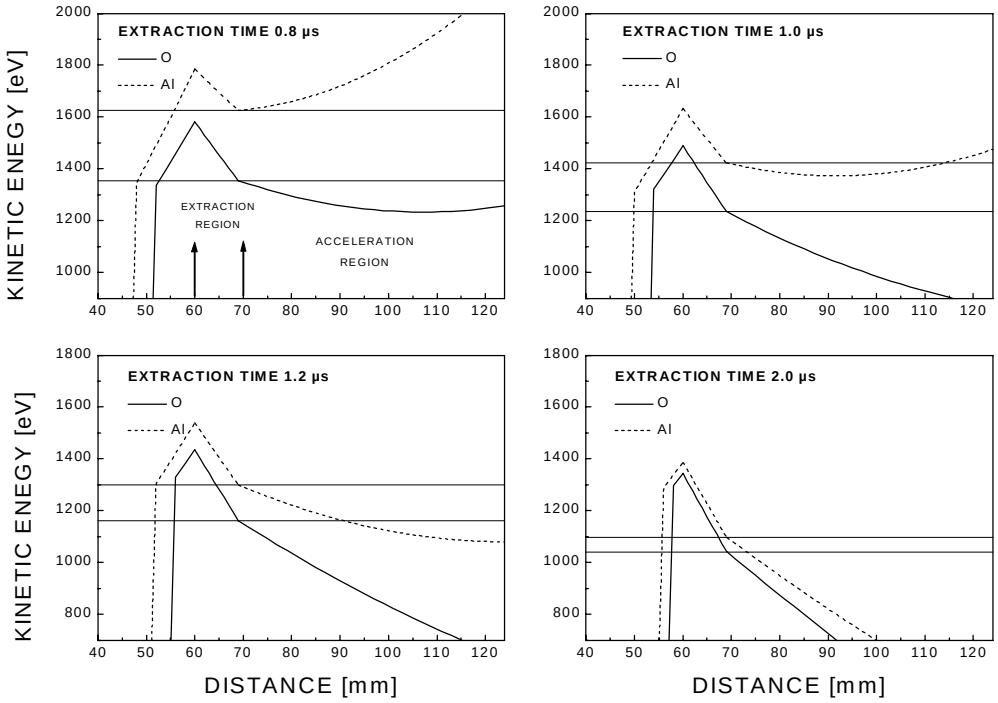

Fig. 2.2-5 Calculated kinetic energies of the particles when reaching the retarding field grid as a function of their position at the moment when the extraction field is applied. The coordinates for the extraction region are between 60 and 70 mm, the acceleration region being between 70 and 130 mm. The horizontal lines represent the used retarding field values.

Detection of neutrals

For the detection of neutrals, a deflecting field (1.5 kV) was used before the extraction region to remove the ions from the plume and let only the neutral particles enter the TOF. A XeCl excimer laser at 308 nm was used as a secondary ionization source for neutral Al ionization in the extraction region (i.e. resonant enhanced multiphoton ionization and hence only Al^0 and no O^0 measurement). The laser was focused in the center of the extraction zone to a spot size of ca 1 mm^2. The number of secondary ionized particles is proportional to the number of neutrals present in the extraction region within the XeCl pulse spatial profile. The delay of the excimer laser pulse was controlled (using a delay unit triggered by the Ti: Sapphire laser pulse) with respect to the femtosecond pulse for constructing the velocity distribution for the neutrals. Since we are detecting particles from a fixed spatial region (the

same argumentation as for the ion measurements holds in this case too), for the velocity distribution representation the detected number of particles as a function of velocity corresponding to the delay time of the ionization source has to be corrected using the temporal neutral yield multiplied with the extraction delay time.

Detection of electrons

For the fast electron detection the sample was negatively biased between 50 and 200V for efficient electron collection. The MSP connections can be externally adjusted for detection of both positively and negatively charged species. For the plume (slow) electrons the TOF spectrometer was used in the Wiley-McLaren configuration with pulsed negative extraction voltages, in an arrangement similar to the ion measurements.

2.3 Experimental procedures

Laser energies

In most of the experiments, unless otherwise stated, the laser fluences for the sub-ps and ps laser pulses were deliberately chosen to be different, but both slightly above the individual ablation threshold, e.g.: 4.0 J/cm^2 for the 0.2 ps regime and 4.3 J/cm^2 for the 2.8 ps regime. The reason for this was to ensure that the fraction of energy above the ablation threshold was about equal in both cases, i.e. to compensate for the pulse-duration dependence of the damage threshold in sapphire [SVR2000]. Naturally, the number of pulses per site also influences the threshold [SVR2000] due to defect formation and to incubation effects (i.e. defect accumulation with increasing number of pulses). However, on the basis of ion-signal threshold studies, the above chosen fluence values make an acceptable compromise.

The laser spot was measured using the properties of a Gaussian spot [Var99]. Since there is a Gaussian distribution of fluences within the Gaussian spot, damage will occur wherever the local fluence exceeds the local threshold. For a range of fluences (minimum two) above the ablation threshold, this can be written as follows.

For $R<R_{damage}$ (where R is the distance from the laser spot center, F is the threshold laser fluence with its threshold value F_{th}, F_1, F_2 (E_1, E_2, respectively) are two experimentally used laser fluences (energies, respectively) corresponding to two different damage areas, S_{laser} is the laser spot area, S_{damage} is the observed damage area):

$$F = \exp\left(-2\frac{\pi R^2}{S_{laser}}\right) \geq F_{th} \text{ with equality for } R=R_{damage} \qquad \text{E 2.3-1}$$

$$\pi R_{damage}^2 = S_{damage}$$

$$F_1 = \exp\left(-2\frac{S_{damage-1}}{S_{laser}}\right) = F_{th}$$

$$F_2 = \exp\left(-2\frac{S_{damage-2}}{S_{laser}}\right) = F_{th}$$

We obtain:

$$\frac{2}{S_{laser}}\left(S_{damage-2} - S_{damage-1}\right) = \ln\left(\frac{F_2}{F_1}\right) = \ln\left(\frac{E_2}{E_1}\right) \qquad \text{E 2.3-2}$$

So the laser spot can be derived from the slope of a dependence similar to the above mentioned functional.

Ablation threshold determination

As will be detailed in the next chapter, the ablation threshold was measured on the basis of the irradiated area modification for a Gaussian profile somewhat similar to the argumentation presented above. Since the damage spot dimensions should depend logarithmically on the laser fluence, the extrapolation of this dependence to zero-modification value will give the ablation threshold. In situ the ablation threshold was checked by observing a burst of ions in the TOF signal.

Pump-probe experiments

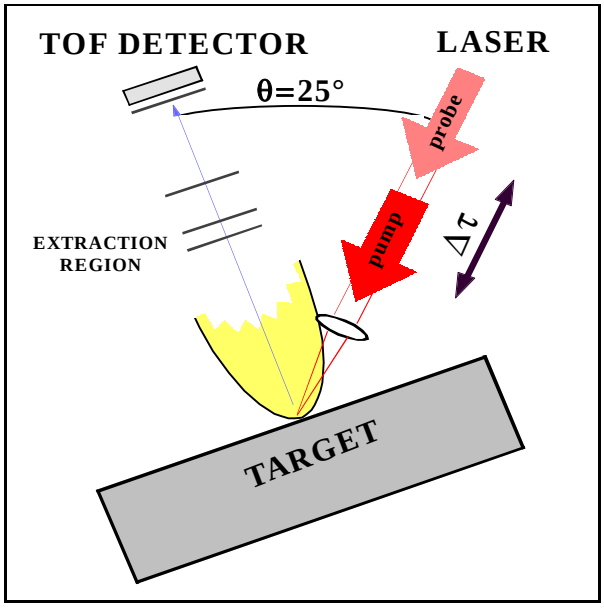

Fig. 2.3-1 Schematic view of the TOF pump-probe experiment.

For the pump-probe experiments the main pulse was split in two beams of controlled energies. In the path of one beam an optical delay line was used, introducing delays in the

range of –300/+300 ps. For the TOF yield detection pump-probe, both pump and probe beams were of equal energies, below the ablation threshold for N=2, minimizing thus the probability of first pulse induced permanent modifications. The signal can be recorded only when there is a correlation between the effects induced by the two pulses, for independent pulses, no ion/electron signal was recorded. A scheme of the experimental arrangement is presented in Fig. 2.3-1.

For the optical scattering measurements a strong pump-pulse (above the threshold) was employed to produce ablation and surface modification. The detected scattered light from a weak probe pulse incident on the pump induced damage spot was detected with a far-field microscope and a photomultiplier (Fig. 2.3-2). The scattered signal increases when the surface topology is altered and constitutes an indication for the onset of ablation. Different polarization directions for pump and probe beams were chosen for better discrimination at the photomultiplier.

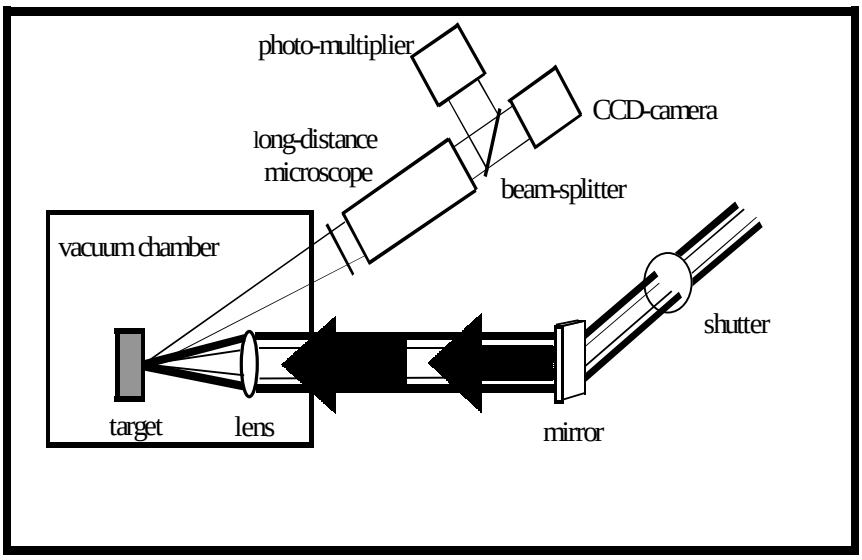

Fig. 2.3-2 Schematic view of the optical scattering experiment.

Plasma light measurements

Measurements on plasma light emission were performed using an imaging setup and a CCD camera. The plume for different conditions of irradiation with respect to the number of shots per site was imaged with a telescopic objective on the active area of a CCD camera allowing also spatial resolution. The results were correlated with the results of other experimental techniques.

Ex-situ investigations

The ex-situ investigations were performed by means of Nomarski interference optical microscopy (Olympus Vanox AHBT3) in both reflection and transmission modes, atomic

force microscopy (Digital Instruments Nanoscope III) in the tapping mode and scanning electron microscopy (Jeol JSM-F). This includes quantitative measurements on the dimensions of the modification area and estimations of the volume of the ablated material.